RSC Advances

PAPER

View Article Online
View Journal | View Issue

Cite this: *RSC Adv.*, 2018, **8**, 23284

Synthesis and characterization of $Ca_3Lu(GaO)_3(BO_3)_4$:Ce^{3+},Tb^{3+} phosphors: tunable-color emissions, energy transfer, and thermal stability

Liangling Sun, Balaji Devakumar, Bin Li, Jia Liang, Heng Guo and Xiaoyong Huang *

Blue-green dual-emitting phosphors $Ca_3Lu(GaO)_3(BO_3)_4$:Ce^{3+},Tb^{3+} (CLGB:Ce^{3+},Tb^{3+}) were synthesized *via* a traditional solid-state reaction method. The phase of the phosphors was characterized by X-ray diffraction and the luminescence properties were investigated using the excitation and emission spectra, decay curves, temperature-dependent emission spectra, CIE chromaticity coordinates, and the internal quantum efficiency. Under 345 nm UV light excitation, Ce^{3+} singly doped CLGB phosphors presented intense blue light in the 350–550 nm wavelength region with a maximum peak at 400 nm. In sharp contrast, CLGB:Ce^{3+},Tb^{3+} phosphors showed both the blue and green emission wavelengths of Ce^{3+} and Tb^{3+} ions, respectively. The overall emission colors can be tuned from blue (0.164, 0.042) to green (0.331, 0.485) *via* increasing the concentration of Tb^{3+} ions, due to the energy transfer (ET) from Ce^{3+} ions to Tb^{3+} ions. The optimal doping concentration of Tb^{3+} ions in CLGB:Ce^{3+},Tb^{3+} phosphors was found to be 40 mol%. The mechanism of the ET from the Ce^{3+} to Tb^{3+} ions was demonstrated to be electric quadrupole–quadrupole interaction. The CLGB:0.04Ce^{3+},0.40Tb^{3+} sample possessed a high IQE of 54.2% and excellent thermal stability with an activation energy of 0.3142 eV when excited at 345 nm. The integrated emission intensity of CLGB:0.04Ce^{3+},0.40Tb^{3+} at 423 K was found to be about 74% of that at 303 K. Finally, under 300 mA driven current, the fabricated prototype white light-emitting diode showed CIE chromaticity coordinates of (0.3996, 0.3856) and high color rending index of 81.2. Considering all the above characteristics, the obtained CLGB:Ce^{3+},Tb^{3+} phosphors can be a type of multicolor emitting phosphor for application in white light-emitting diodes.

Received 17th April 2018
Accepted 29th May 2018

DOI: 10.1039/c8ra03289k

rsc.li/rsc-advances

1. Introduction

Nowadays, environmental and energy issues are attracting increasing attention, so resource-saving and environment-friendly industries are valued.[1–4] In the lighting industry, white light-emitting diodes (w-LEDs) have many advantages in lighting applications, such as having long working lifetimes and high luminous efficiency, and being energy-saving and environment-friendly, which meet the requirements of saving energy and protecting the environment.[5–10] At present, two methods have been used to fabricate the w-LEDs; one is combining a blue InGaN chip with commercial yellow phosphor $Y_3Al_5O_{12}$:Ce^{3+}, and the other is using an ultraviolet/near ultraviolet (n-UV; 350–420 nm) LED chip and tricolor (red, green, and blue) phosphors.[11–16] The former one suffers from low color rendering index and high correlated color temperature, while the latter one has the drawback of adjusting the proportion of the tricolor phosphors in particular applications.[17] In fact, the luminescence properties of the w-LEDs based on the tricolor phosphors are greatly affected by the mixing degree, so it is important to explore novel phosphor with single phase to meet the requirement of practical application in w-LEDs.

Many rare-earth ions co-doped luminescent inorganic phosphors have been studied due to the energy transfer between a sensitizer (*e.g.*, Dy^{3+} and Ce^{3+}) and an activator (*e.g.*, Tb^{3+} and Sm^{3+}), which can broaden the excitation wavelength range and enhance the luminescence performance.[18–23] Tb^{3+} ions are frequently used as an activator because it can give rise to green light at about 541 nm ($^5D_4 \rightarrow {}^7F_5$ transition).[24–26] However, Tb^{3+} ions exhibits a narrow weak band in the n-UV region, because of the spin-forbidden 4f → 4f transitions. On the contrary, Ce^{3+} ions could show a strong and broad absorption band in the n-UV region when it is doped into particular compounds, owing to the 4f → 5d parity-allowed transition.[27,28] Thus considering this situation, Ce^{3+} ions can be used as sensitizer to intensify Tb^{3+} ions absorption by ET from Ce^{3+} to Tb^{3+} ions. Previous studies have shown that Ce^{3+} and Tb^{3+} ions can be well co-doped into various inorganic compounds, such

Key Lab of Advanced Transducers and Intelligent Control System, Ministry of Education and Shanxi Province, College of Physics and Optoelectronics, Taiyuan University of Technology, Taiyuan 030024, PR China. E-mail: huangxy04@126.com

as $Na_3Sc_2(PO_4)_3$:Ce^{3+},Tb^{3+},[29] $Ba_2Y_3(SiO_4)_3F$:Ce^{3+},Tb^{3+},[30] $LaSi_3N_5$:Ce^{3+},Tb^{3+},[31] and $Na_6Ca_3Si_6O_{18}$:Ce^{3+},Tb^{3+}.[32] But few papers have studied the effect of temperature on luminescence. In these articles that have reported the thermal stability, such as $CaLa_4Si_3O_{13}$:Ce^{3+},Tb^{3+} and $BaLu_6(Si_2O_7)_2(Si_3O_{10})$:$Ce^{3+}$,$Tb^{3+}$, their luminous intensity remained about 70% and 71.5% at 423 K compared with the initial value at 303 K, respectively, which was lower than the value of 74% in this present paper.[27,33]

Borates activated by rare-earth ions, such as $LaBWO_6$:Tb^{3+},Eu^{3+},[34] ZnB_4O_7:Eu^{3+},[35] $Ba_2B_2O_5$:Ce^{3+},Tb^{3+},Sm^{3+},[36] have been confirmed to be an important class of phosphors with low synthesis temperature and high luminescence efficiency.[37–39] In this paper, $Ca_3Lu(GaO)_3(BO_3)_4$ (CLGB) had been selected to be the host material and Ce^{3+}–Tb^{3+} co-activated CLGB phosphors were prepared. The luminescence properties, thermal stability, the critical distance, chromaticity parameters, and ET mechanism between the Ce^{3+} and Tb^{3+} ions were systematically investigated. Importantly, the adjustable color from blue to green were achieved by doping various concentrations of the Tb^{3+} ions, due to the ET from Ce^{3+} to Tb^{3+} ions. Finally, a prototype w-LED device was fabricated by using a 365 nm UV LED chip and the phosphor mixture of CLGB:Ce^{3+},Tb^{3+} green phosphors, $BaMgAl_{10}O_7$:Eu^{2+} blue phosphors, and $CaAlSiN_3$:Eu^{2+} red phosphors.

2. Experimental

The target materials of CLGB:Ce^{3+},Tb^{3+} phosphors were synthesized by high-temperature solid-state reaction method. H_3BO_3 (analytical reagent, AR), $CaCO_3$ (AR), Ga_2O_3 (AR), Lu_2O_3 (99.99%), CeO_2 (99.99%), and $Tb(NO_3)_3\cdot 6H_2O$ (99.99%) were served as the raw materials and they were weighted according to stoichiometric ratio while H_3BO_3 exceeded 5 wt%. The raw materials were ground and mixed in an agate mortar. Then, these mixtures were sintered at 1000 °C for 4 h in CO reducing atmosphere to reduce the Ce^{4+} into Ce^{3+} ions and prevent Ce^{3+} ions from being re-oxidized to Ce^{4+} ion at high temperature. Finally, the prepared mixtures were cooled naturally to room temperature in the furnace.

The XRD patterns of CLGB:Ce^{3+},Tb^{3+} were examined by Bruker D8 X-ray diffractometer. The morphology properties of the CLGB:0.04Ce^{3+},0.40Tb^{3+} phosphors were measured by a field-emission scanning electron microscope (FE-SEM; MAIA3 TESCAN). The diffuse reflectance spectra (DRS) were recorded on a spectrophotometer (Shimadzu 2600UV) using $BaSO_4$ white powder as the reference. The photoluminescence (PL) and PL excitation (PLE) spectra were researched by Edinburgh FS5 fluorescence spectrophotometer equipped with a 150 W Xe lamp as the excitation light source. The thermal stability and internal quantum efficiency (IQE) of CLGB:0.04Ce^{3+},0.40Tb^{3+} phosphors were measured on the same spectrophotometer equipped with an temperature-regulating device and an integrating sphere coated with $BaSO_4$ compound, respectively. The luminescence decay curves of Ce^{3+} ions were measured by utilizing an Edinburgh FPS 920 spectrofluorometer with a 150 W nF900 nanosecond flash-light source. The CLGB:0.04Ce^{3+},0.40Tb^{3+} phosphors, commercial blue emitting phosphors $BaMgAl_{10}O_7$:Eu^{2+}, and red emitting phosphors $CaAlSiN_3$:Eu^{2+} were mixed thoroughly and then coated on a 365 nm LED chip by using silicone to fabricate w-LED device. The photoelectric properties and spectral power distributions of the fabricated devices were measured by using an integrating sphere spectroradiometer system (HAAS-2000, Everfine) and a corrected spectrometer, respectively.

3. Results and discussion

The XRD patterns of the CLGB:0.04Ce^{3+}, CLGB:0.04Ce^{3+},0.40Tb^{3+} phosphors, and the stand cards of $Ca_3Y(GaO)_3(BO_3)_4$ (ICSD-172155) and $LuBO_3$ (JCPDS-13-0481) were shown in Fig. 1(a). The standard curve of $Ca_3Y(GaO)_3(BO_3)_4$ host and the dominant diffraction peaks of CLGB:0.04Ce^{3+} and CLGB:0.04Ce^{3+},0.40Tb^{3+} phosphors were well-matched, which indicated the formation of CLGB:Ce^{3+},Tb^{3+} phosphors and the iso-structure of CLGB:Ce^{3+},Tb^{3+} phosphors and the $Ca_3Y(GaO)_3(BO_3)_4$ material. There was a week miscellaneous peak centered at $2\theta \approx 27°$, which was derived from $LuBO_3$ (JCPDS: 13-0481). However, the impurity week peak decreased with the addition of Tb^{3+} ions, which implied that the pure phase CLGB:Ce^{3+},Tb^{3+} samples could be obtained by doping high concentration of Tb^{3+} ions in CLGB host. Fig. 1(b) depicted the Rietveld refinements of the CLGB:0.04Ce^{3+},0.40Tb^{3+} phosphors to further study the crystal structure of the as-prepared sample, and the crystallographic file and refinement parameters of CLGB:0.04Ce^{3+},0.40Tb^{3+} phosphors were listed in Table 1. It could be found that the CLGB:0.04Ce^{3+},0.40Tb^{3+} phosphors possessed a hexagonal space group $P6_3/m$ based on the refinement results from Table 1. The crystal structure of CLGB:0.04Ce^{3+},0.40Tb^{3+} phosphors and the local environment of the Ca1 and Ca2 sites were showed in Fig. 1(c) and (d), respectively. From the Table 1 and Fig. 1(d), we could know that even though the Ca2 was surrounded by ten oxygen atoms, the Lu^{3+}, Ce^{3+}, and Tb^{3+} would prefer to occupy the Ca1 site which coordinated by seven oxygen atoms. That was because the four O4 ions which surrounded the Ca2 was shared by the adjacent four B ions. Therefore, the Lu^{3+}, Ce^{3+}, and Tb^{3+} ions would occupy the Ca1 with the CN sites of 9 (CN: coordination number), not the Ca2 with the CN sites of 7.[40]

The FE-SEM of the CLGB:0.04Ce^{3+},0.40Tb^{3+} phosphors were measured and showed in Fig. 2. It could be seen that the CLGB:0.04Ce^{3+},0.40Tb^{3+} phosphors were made up of irregular and agglomerate microparticles with the size ranging from 2 to 8 μm.

Fig. 3(a) illustrated the PLE and PL spectra of CLGB:0.04Ce^{3+}. The PLE spectrum monitored at 400 nm showed a weak excitation band peaking at 281 nm from 250–300 nm wavelength region and an intense broad excitation band peaking at 345 nm from 300–392 nm wavelength region, which were assigned to 4f–5d transition of Ce^{3+} ions in CLGB:0.04Ce^{3+} phosphors.[41,42] Importantly, the broad excitation band from 300 to 392 nm matched well with the emission spectra of n-UV LED chips.[43] The PL spectrum of CLGB:0.04Ce^{3+} showed an asymmetric blue emission band (contain 5d → $^2F_{5/2}$ and 5d → $^2F_{7/2}$ transitions) from 350 to 550 nm and it could be separate into two different

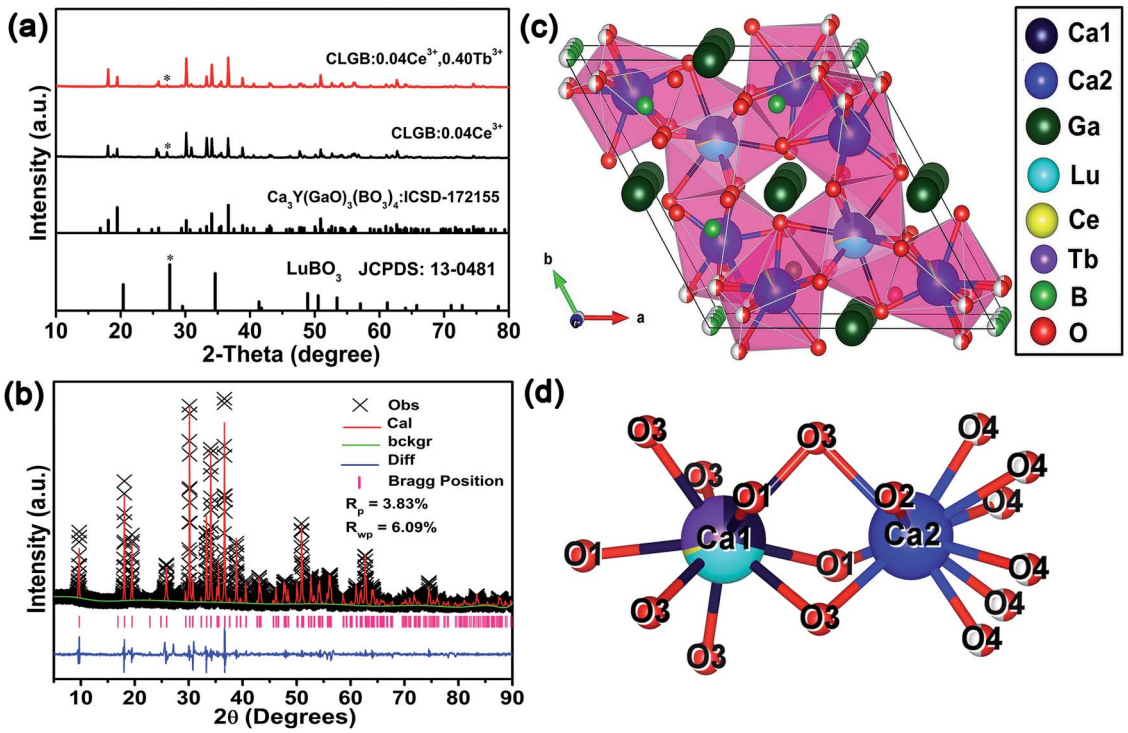

Fig. 1 (a) XRD patterns of CLGB:0.04Ce^{3+} and CLGB:0.04Ce^{3+},0.40Tb^{3+} phosphors. The standard cards of $Ca_3Y(GaO)_3(BO_3)_4$ (ICSD: 172155) and $LuBO_3$ (JCPDS: 13-0481) were also shown as the references. (b) Rietveld refinements of the XRD files for CLGB:0.04Ce^{3+},0.4Tb^{3+} phosphors. (c) The crystal structure of CLGB:0.04Ce^{3+},0.4Tb^{3+} phosphors. (d) The local environment of the Ca1 and Ca2 sites.

Gaussian peaks, peaking at 385 nm (25 974 cm^{-1}) and 409 nm (24 450 cm^{-1}).[44,45] Therefore, the energy difference of the two Gaussian peaks was about 1524 cm^{-1}, which was in agreement with the theoretical difference between the $^2F_{5/2}$ and $^2F_{7/2}$ levels of Ce^{3+} ions (about 2000 cm^{-1}).[46,47]

Fig. 3(b) shows the PLE and PL spectra of CLGB:0.40Tb^{3+}. In the PLE spectrum monitored the emission at 544 nm, a broad excitation band in the range of 200–300 nm and a group of narrow PLE lines in the 300–400 nm wavelength range were observed, corresponding to $4f^8 \rightarrow 4f^75d^1$ transition and $4f^8$–$4f^8$ transitions of Tb^{3+} ions, respectively.[25] Furthermore, the CLGB:0.40Tb^{3+} phosphors showed green emissions under 370 nm n-UV light excitation. The PL spectrum of CLGB:0.40Tb^{3+} displayed several emission peaks at 492 nm ($^5D_4 \rightarrow {}^7F_6$ transition), 544 nm ($^5D_4 \rightarrow {}^7F_5$ transition), 585 nm ($^5D_4 \rightarrow {}^7F_4$ transition), and 621 nm ($^5D_4 \rightarrow {}^7F_3$ transition).[48,49]

According to Dexter's theory, effective ET between activator and sensitizer need to meet two conditions: (1) the PL spectrum of the sensitizer (herein was Ce^{3+} ions) and the PLE spectrum of the activator (herein was Tb^{3+} ions) had enough overlap; (2) when monitored at the dominant emission wavelength of the activator, the PLE spectrum of the co-doped sample (herein was CLGB:Ce^{3+},Tb^{3+}) should have not only the characteristic excitation bands of the activator ions but also the characteristic

Table 1 The parameters from Rietveld refinement of the CLGB:0.04Ce^{3+},0.40Tb^{3+} sample

CLGB:0.04Ce^{3+},0.40Tb^{3+}					
Crystal system	Hexagonal				
Space group	$P6_3/m$				
Lattice parameters	a = 10.50796(11) Å, b = 10.50796 Å, c = 5.81483(10) Å, $\alpha = \beta = 90°$, $\gamma = 120°$, V = 556.038(10) Å^3				
Atom	x	y	z	Occ.	U_{iso} (Å^2)
Ca1/Lu1/Ce1/Tb1	0.3333	0.6667	0.25	0.29/0.4/0.025/0.3	0.011
Ca2/Lu2/Ce2/Tb2	0.1264	0.8414	0.25	0.905/0.016/0.015/0.1	0.014
Ga1	0.0	0.5	0.0	1	0.012
B1	0.17543	0.81737	0.75	1	−0.04826
B2	0.0	0.0	0.117	0.5	0.02
O1	0.05155	0.43126	0.25	1	0.02272
O2	0.331	0.915	0.75	1	0.018
O3	0.3021	0.477	0.539	1	0.012
O4	0.053	0.907	0.587	0.5	0.005

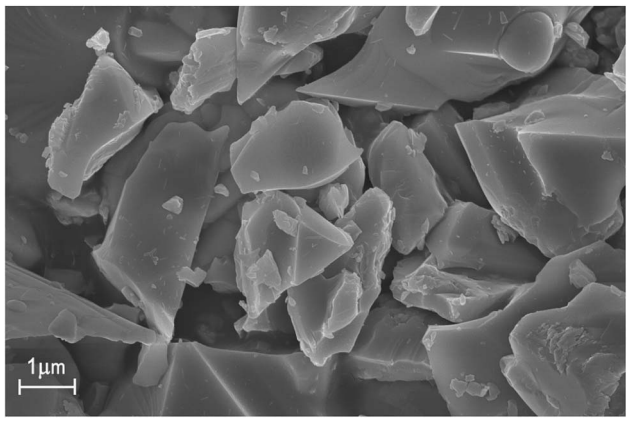

Fig. 2 The FE-SEM image of the CLGB:0.04Ce^{3+},0.40Tb^{3+} phosphors.

excitation peaks of the sensitizer ions.[50–52] By comparing Fig. 3(a) and (b), it was obvious that the PLE spectrum of CLGB:0.40Tb^{3+} had large overlap with the PL spectrum of CLGB:0.04Ce^{3+} between 348 and 400 nm, which met the requirement of the resonance-type ET. Furthermore, as shown in Fig. 3(c), the PLE spectrum of CLGB:0.04Ce^{3+},0.40Tb^{3+} monitored at 544 nm (Tb^{3+} dominant emission peak) have two kind of excitation bands: the broad PLE bands in the 252–380 nm wavelength region were the characteristic excitation bands of Ce^{3+} ions, while a broad PLE band in the 232–252 nm region ($4f^8 \rightarrow 4f^7 5d^1$ transition) and several sharp PLE peaks in the 366–390 nm wavelength range ($4f^8$–$4f^8$ transitions) belonged to the Tb^{3+} ions. In contrast, when monitored at Ce^{3+} dominant emission peak at 400 nm, the PLE spectrum of CLGB:0.04Ce^{3+},0.40Tb^{3+} phosphors only displayed the characteristic excitation bands of Ce^{3+} ions. These results indicated the occurrence of ET from Ce^{3+} to Tb^{3+} ions in CLGB:0.04Ce^{3+},0.40Tb^{3+}. Meanwhile, compared the PLE spectra of CLGB:0.40Tb^{3+} and CLGB:0.04Ce^{3+},0.40Tb^{3+}, we could concluded that the absorption intensity in the n-UV region of Tb^{3+} ions was enhanced with the addition of Ce^{3+} ions. Under UV light excitation at 345 nm, the PL spectrum of CLGB:0.04Ce^{3+},0.40Tb^{3+} displayed the characteristic emission bands of Ce^{3+} and Tb^{3+} ions, further showing the presence of ET from Ce^{3+} to Tb^{3+} ions in CLGB:Ce^{3+},Tb^{3+} phosphors.

Fig. 4 showed the DRS of the CLGB host, CLGB:0.04Ce^{3+}, and CLGB:0.04Ce^{3+},0.40Tb^{3+} phosphors. Compared with the spectral curve of the CLGB host, it could be clearly seen from the spectrum of CLGB:0.04Ce^{3+} phosphors that two new absorption bands in 270–400 nm appeared, which might be attributed to the 4f → 5d transition of Ce^{3+} ions. For the DRS of CLGB:0.04Ce^{3+},0.40Tb^{3+} phosphors, another absorption peak at 250 nm was observed due to the $4f^8 \rightarrow 4f^7 5d^1$ transition of Tb^{3+}.[25] These results obtained from the DRS were well accordance with the PLE spectra in Fig. 3.

To find the optimal doping concentration of Ce^{3+} ions in CLGB host, a series of Ce^{3+} ions single doped CLGB phosphors were synthesized and the PL spectra excited at 345 nm were shown in Fig. 5. The emission intensity of CLGB:$x$$Ce^{3+}$ (x = 0.005–0.060) reached the maximum at x = 0.04. Therefore, the co-doping concentration of Ce^{3+} ions was fixed to be 0.04 and then a series of CLGB:0.04Ce^{3+},$y$$Tb^{3+}$ (y = 0.00–0.50) phosphors were synthesized and the corresponding PL spectra excited at 345 nm were shown in Fig. 6(a). With the increasing doping concentration of Tb^{3+} ions in CLGB:0.04Ce^{3+},$y$$Tb^{3+}$ (y = 0.00–0.50) phosphors, the emission intensity of Ce^{3+} ions gradually decreased and the emission intensity of Tb^{3+} ions markedly

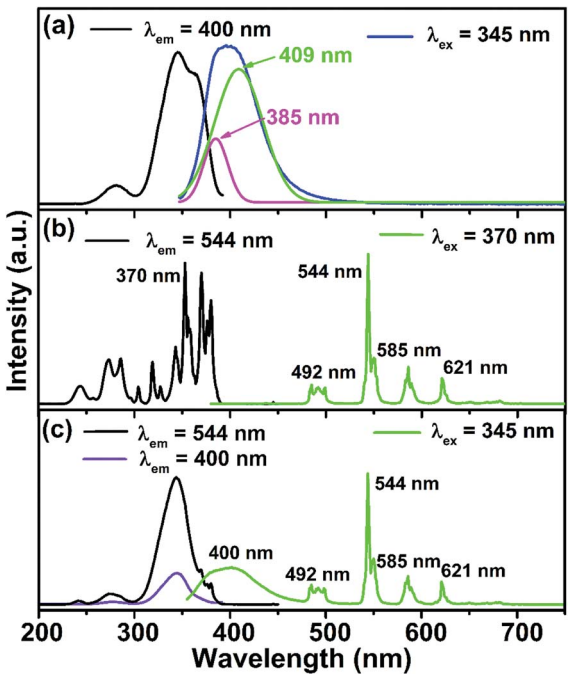

Fig. 3 The PLE and PL spectra of CLGB:0.04Ce^{3+} (a), CLGB:0.40Tb^{3+} (b), and CLGB:0.04Ce^{3+},0.40Tb^{3+} (c) phosphors.

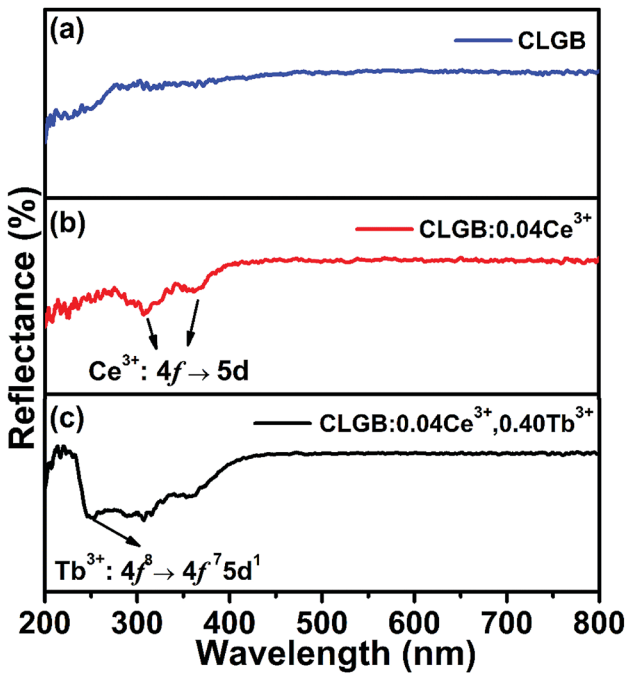

Fig. 4 The DRS of (a) CLGB host, (b) CLGB:0.04Ce^{3+}, and (c) CLGB:0.04Ce^{3+},0.40Tb^{3+} samples.

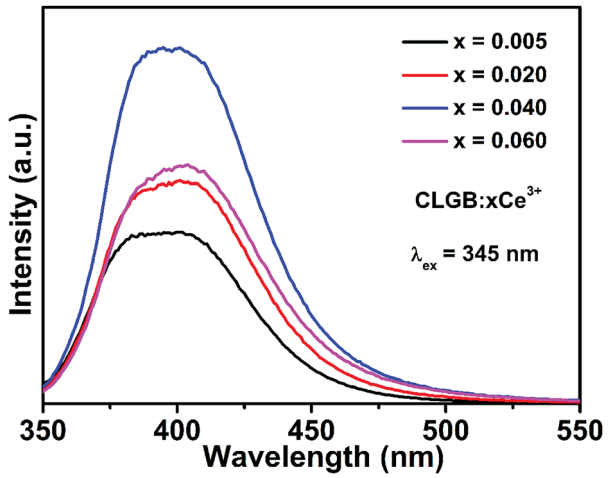

Fig. 5 The PL spectra for CLGB:xCe^{3+} (x = 0.005–0.060) phosphors.

enhanced, as can be clearly seen in Fig. 6(a) and (b). Especially, Tb^{3+} green emission intensity reached the maximum when y = 0.40. This phenomenon illustrated that there existed effective ET from Ce^{3+} to Tb^{3+} ions in CLGB:0.04Ce^{3+},$y$$Tb^{3+}$ phosphors and the emission intensity of blue light (355–475 nm) and the green light (475–700 nm) could be tuned by doping different concentration of Tb^{3+} ions. The ET efficiency (η_{ET}) from Ce^{3+} sensitizers to Tb^{3+} activators in CLGB:0.04Ce^{3+},$y$$Tb^{3+}$ phosphors can be calculated by:[53,54]

$$\eta_{ET} = 1 - \frac{I_s}{I_{s0}} \quad (1)$$

where I_{s0} and I_s are the PL intensity of the Ce^{3+} sensitizers without and with the presence of Tb^{3+} ions, respectively. Based on the eqn (1), the results were measured and listed in Fig. 6(b). It could be clearly seen that the η_{ET} gradually increased with the increasing Tb^{3+} ions content and reached 67.4% when y = 0.50, which indicated effective ET from Ce^{3+} to Tb^{3+} ions in CLGB:0.04Ce^{3+},$y$$Tb^{3+}$ phosphors.

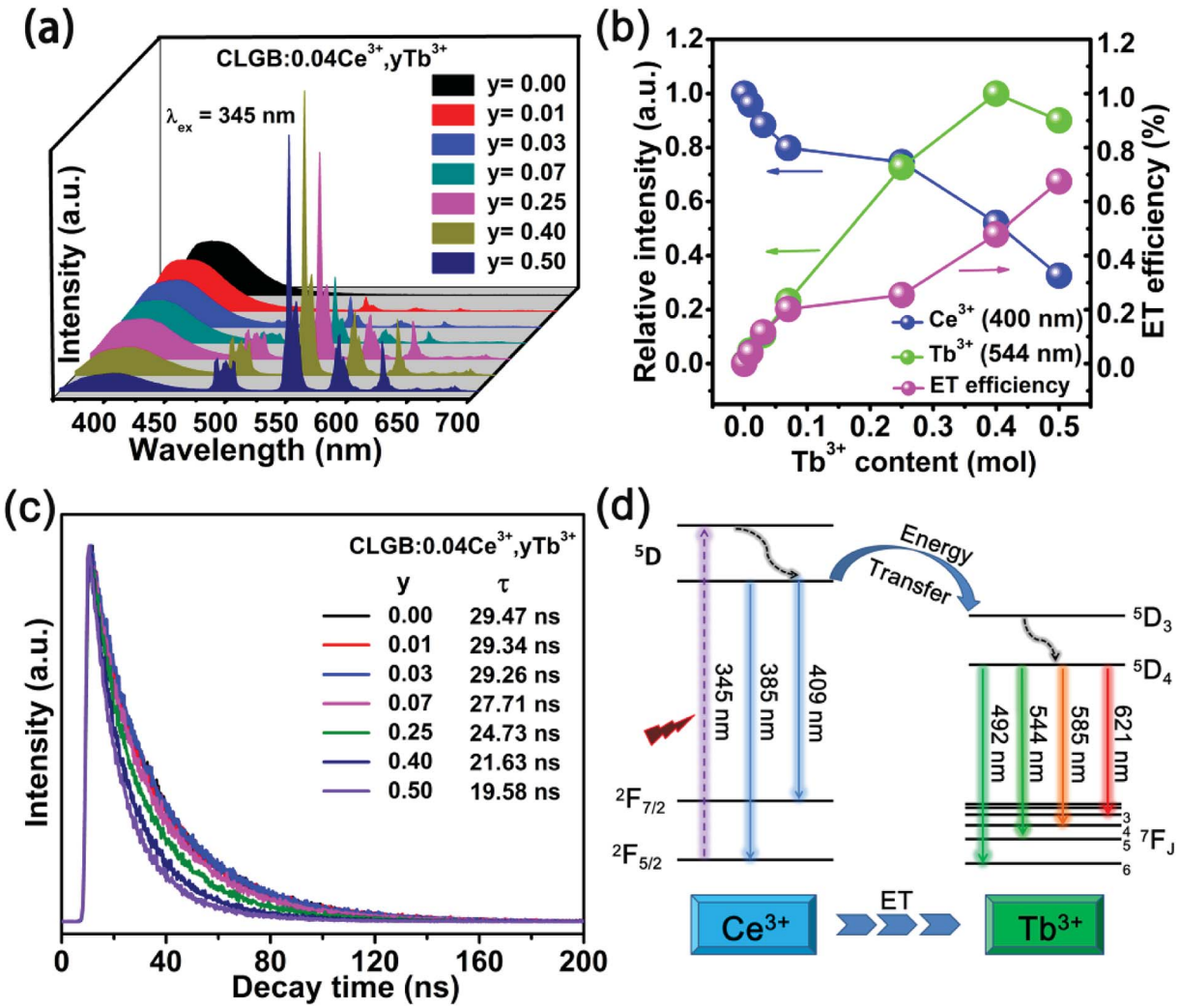

Fig. 6 (a) The content-dependent PL of CLGB:0.04Ce^{3+},$y$$Tb^{3+}$ (y = 0.00–0.50). (b) The dependences of Ce^{3+} 400 nm emission intensity, Tb^{3+} 544 nm emission intensity, and the ET efficiency from Ce^{3+} to Tb^{3+} ions on the doping concentrations of Tb^{3+} ions for CLGB:0.04Ce^{3+},$y$$Tb^{3+}$ (y = 0.00–0.50) phosphors. (c) Decay curves of Ce^{3+} ions in CLGB:0.04Ce^{3+},$y$$Tb^{3+}$ (y = 0.00–0.50) samples. (d) Energy level diagram shows the emission mechanism of CLGB:Ce^{3+},Tb^{3+} and the ET process.

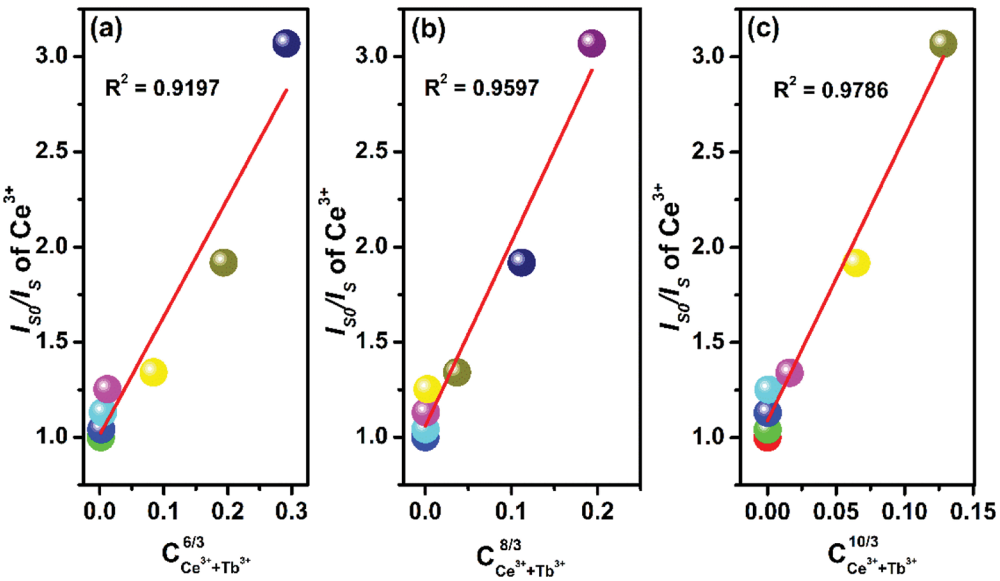

Fig. 7 Dependence of I_{s0}/I_s of Ce^{3+} ions on (a) $C(Ce^{3+} + Tb^{3+})^{6/3}$, (b) $C(Ce^{3+} + Tb^{3+})^{8/3}$, and (c) $C(Ce^{3+} + Tb^{3+})^{10/3}$.

The decay curves of Ce^{3+} ions in CLGB:0.04Ce^{3+},yTb^{3+} phosphors were measured under 345 nm excitation, as shown in Fig. 6(c). The decay lifetimes were measured by the following double exponential expression:[55]

$$I = A_1 \exp\left(-\frac{t}{\tau_1}\right) + A_2 \exp\left(-\frac{t}{\tau_2}\right) \quad (2)$$

where t is time and I is luminescence intensity; τ_1 and τ_2 are the exponential components of lifetimes; A_1 and A_2 are constants. It can be clearly seen from Fig. 6(c) that the average decay lifetimes τ gradually decreased from 29.47 to 19.58 ns when the concentration of Tb^{3+} ions (y) increased from 0.00 to 0.50, which was the strong evidence of the occurrence of ET from Ce^{3+} to Tb^{3+} ions in CLGB:0.04Ce^{3+},yTb^{3+} phosphors.

Fig. 6(d) shows a schematic diagram for the ET process from Ce^{3+} to Tb^{3+} ions in CLGB:Ce^{3+},Tb^{3+} phosphors. Excited by the 345 nm excitation, electrons in the ground state $^2F_{5/2}$ of Ce^{3+} ions absorbed energy and then were excited to the excited higher 5d level and finally returned to the lower level of 5d excited state. After that there was two ways for energy releasing. (1) Transitions of Ce^{3+} ions: a partial of excited electrons released to lower 4f level and gave rise to blue emissions at 385 and 409 nm.[56] (2) ET process from Ce^{3+} to Tb^{3+} ions: other partial excited energy of Ce^{3+} ions could be transferred to the $^5D_3$ level of Tb^{3+} ions due to their similar energy levels.[57,58] After that, the excited electrons on the $^5D_3$ energy level will relax to the $^5D_4$ level by non-radiative transitions and then emitted green light at 492, 544, 585, and 621 nm by radiative transitions of $^5D_4 \rightarrow {}^7F_{6,5,4,3}$.

In general, the ET from a sensitizer to an activator in certain phosphor may take place *via* exchange interaction and electric multipolar interaction.[56] For the exchange interaction, the critical distance (R_c) between the doping ions (herein were the Ce^{3+} and Tb^{3+} ions) should be smaller than 5 Å and it can be obtained by the follow equation:[59,60]

$$R_c = 2\left(\frac{3V}{4\pi x_c N}\right)^{\frac{1}{3}} \quad (3)$$

where V is the volume of the unit cell, x_c is the total optimal concentration of the doping ions in co-doped phosphors, and N is the number of sites in the unit cell that can be substituted by the doping ions. For the CLGB:0.04Ce^{3+},0.40Tb^{3+} phosphors, V

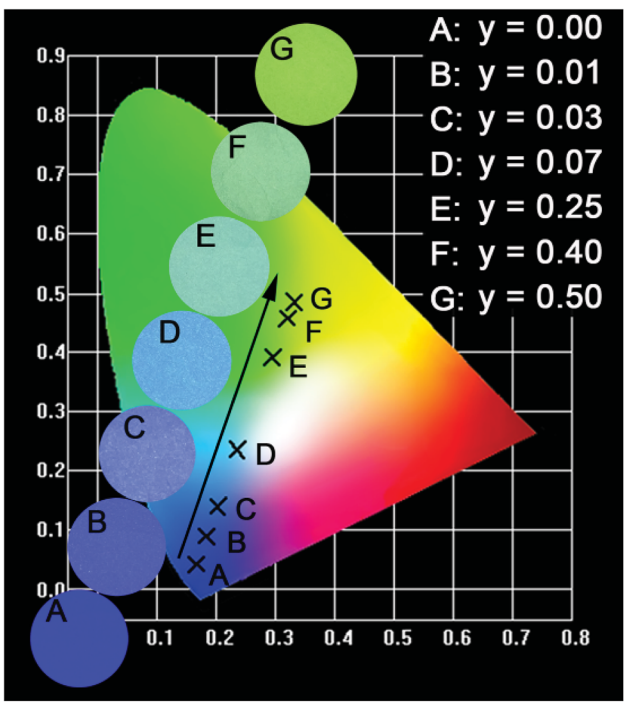

Fig. 8 CIE chromaticity coordinates for CLGB:0.40Ce^{3+},yTb^{3+} phosphors and digital photos of corresponding samples under 365 nm UV lamp.

Table 2 The CIE chromaticity coordinates (x, y) and IQEs for CLGB:0.04Ce^{3+},yTb^{3+} phosphors under 345 nm excitation

Sample	Tb^{3+} concentration (y)	CIE coordinates (x, y)	IQE (%)
A	0.00	(0.164, 0.042)	45.1
B	0.01	(0.182, 0.090)	46.3
C	0.03	(0.201, 0.140)	46.3
D	0.07	(0.234, 0.235)	46.5
E	0.25	(0.294, 0.391)	57.9
F	0.40	(0.320, 0.458)	54.2
G	0.50	(0.331, 0.485)	38.7

$= 556.038$ Å^3, $N = 2$, $x_c = 0.44$, thus R_c was calculated to be about 10.65 Å. Because of the value of $R_c > 5$ Å, so the ET process occurred by electric multipolar interaction.[52] Since there were three forms of the electric multipolar interaction, so the specific form of ET process can be given by the following expression:[61,62]

$$\frac{\eta_0}{\eta_s} \propto C^{\frac{n}{3}} \quad (4)$$

where η_0 and η_s represent the luminescence quantum efficiencies of Ce^{3+} ions in the absence and presence of Tb^{3+} ions, respectively. C is the sum of the concentration of Ce^{3+} and Tb^{3+} ions. The values of $n = 6$, 8 and 10 represent the electric dipole–dipole (d–d), dipole–quadrupole (d–q) and quadrupole–quadrupole (q–q) interactions, respectively.[63] The value η_0/η_s can be replaced by I_{s0}/I_s for an approximate value, which make the exp. (4) described as following:[62]

$$\frac{I_{s0}}{I_s} \propto C^{\frac{n}{3}} \quad (5)$$

Herein, I_{s0} and I_s represent the PL intensities of CLGB:0.04Ce^{3+} and CLGB:0.04Ce^{3+},yTb^{3+} (y = 0.01–0.50) phosphors, respectively. The I_{s0}/I_s as a function of $C^{n/3}$ was illustrated in Fig. 7. By compared the fitting result R^2 which represents the fitting correlation, the maximum value reached when $n = 10$ (see Fig. 7(c)), implying that the primary ET mechanism from Ce^{3+} to Tb^{3+} ions in CLGB:$x$$Ce^{3+}$,$yTb^{3+}$ phosphors was electric q–q interaction.

Based on the PL spectra, the CIE chromaticity diagram of CLGB:0.04Ce^{3+},yTb^{3+} (y = 0–0.50) was depicted in Fig. 8, and the corresponding CIE coordinates were listed in Table 2. The sample color and CIE coordinates of CLGB:0.04Ce^{3+},yTb^{3+} shifted gradually from blue [$y = 0.00$, CIE:(0.164, 0.042)] to green [$y = 0.50$, CIE:(0.331, 0.485)] by adjusting Tb^{3+} ions concentration from 0.00 to 0.50. Table 2 also shows the IQEs of the CLGB:0.04Ce^{3+},yTb^{3+} (y = 0.00–0.50) phosphors. The IQE of the obtained CLGB:0.04Ce^{3+},yTb^{3+} (y = 0.00–0.50) phosphors reached its maximum value of 57.9 when $y = 0.25$. To evaluate

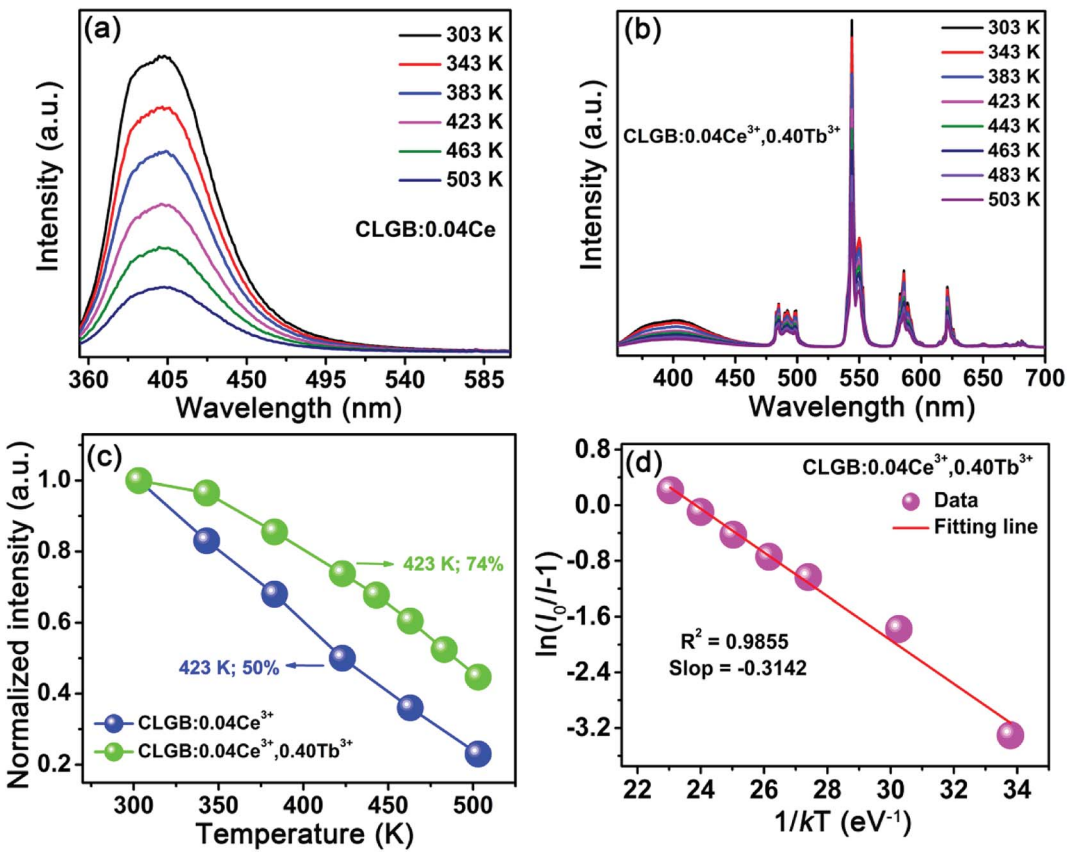

Fig. 9 Temperature-dependent PL spectra (λ_{ex} = 345 nm) of (a) CLGB:0.04Ce^{3+} and (b) CLGB:0.04Ce^{3+},0.40Tb^{3+} phosphors. (c) Normalized PL intensities of CLGB:0.04Ce^{3+} and CLGB:0.04Ce^{3+},0.40Tb^{3+} phosphors as a function of sample temperature under 345 nm excitation. (d) Plots of $\ln(I_0/I - 1)$ *versus* $1/kT$ of the CLGB:0.04Ce^{3+},0.40Tb^{3+} phosphors.

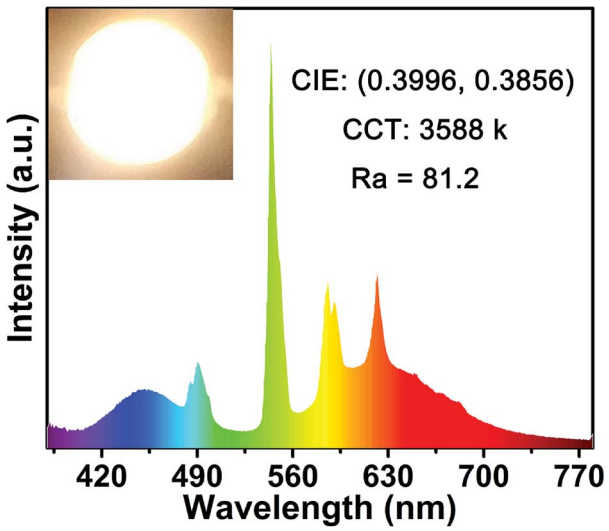

Fig. 10 EL spectrum of the fabricated w-LED device consisting of 365 nm n-UV chip, CLGB:0.04Ce^{3+},0.40Tb^{3+} green emitting phosphors, $BaMgAl_{10}O_7$:Eu^{2+} blue emitting phosphor and $CaAlSiN_3$:Eu^{2+} red emitting phosphors.

the application possibility in w-LEDs of the CLGB:Ce^{3+},Tb^{3+} compounds, thermal stability is an important technological parameter. The temperature-dependent PL spectra of Ce^{3+} singly-doped CLGB:0.04Ce^{3+} and Ce^{3+}–Tb^{3+} co-doped CLGB:0.04Ce^{3+},0.40Tb^{3+} phosphors were measured and plotted in Fig. 9(a) and (b), respectively. Clearly, the PL intensities of CLGB:0.04Ce^{3+} and CLGB:0.04Ce^{3+},0.40Tb^{3+} phosphors decreased with the increasing temperature and they were dropped about 50% (remained 50%) and 26% (remained 74%) at 423 K of that measured at 303 K, respectively (see Fig. 9(c)). Importantly, the thermal stability of the CLGB:0.04Ce^{3+},0.40Tb^{3+} phosphors was better than the CLGB:0.04Ce^{3+} phosphors. Considering the good thermal performance, the activation energy (ΔE) for the thermal quenching of CLGB:0.04Ce^{3+},0.40Tb^{3+} phosphors can be calculated by following Arrhenius equation:[64–66]

$$I(T) = I_0\left[1 + c\exp\left(-\frac{\Delta E}{kT}\right)\right]^{-1} \quad (6)$$

where I_0 and I are the integrated intensities at room temperature (303 K) and various measurement temperatures from 303–503 K, respectively. The parameters C, k and T represent a constant, the Boltzmann constant (8.629×10^{-5} eV K^{-1}) and the given temperature, respectively. According to eqn (6), The $\ln(I_0/I - 1)$ *versus* $1/(kT)$ of CLGB:0.04Ce^{3+},0.40Tb^{3+} was plotted and shown in Fig. 9(d). It can be seen that the value of the ΔE of the CLGB:0.04Ce^{3+},0.40Tb^{3+} phosphors was 0.3142 eV, which was higher than that of $BaLu_6(Si_2O_7)_2(Si_3O_{10})$:$Ce^{3+}$,$Tb^{3+}$ phosphors ($\Delta E = 0.25055$ eV).[33]

Considering the good thermal performance and high IQE, the research of the fabricate w-LED device was meaningful. Fig. 10 shows the electroluminescent (EL) spectrum of the as-prepared w-LED device. The device exhibited bright white light with CIE chromaticity coordinates of (0.3996, 0.3856), high color rending index (Ra) of 81.2 and correlated color temperature (CCT) of 3588 K. Thus, all the above results show that the CLGB:Ce^{3+},Tb^{3+} phosphors have good properties to meet the requirements of practical application in w-LEDs.

4. Conclusions

In summary, novel CLGB:Ce^{3+},Tb^{3+} phosphors were successfully synthesized by solid-state reaction at 1000 °C. Fixed the Ce^{3+} ions concentration $x = 0.04$, the CLGB:0.04Ce^{3+},yTb^{3+} (y = 0.01–0.50) samples exhibited blue emission (355–475 nm) and green emission (475–700 nm) under 345 nm excitation. ET from the Ce^{3+} to Tb^{3+} ions was observed in CLGB:0.04Ce^{3+},yTb^{3+} phosphors and the ET process occurred by electric q–q interaction. By adjusting the Tb^{3+} ions concentration, the emission color of the CLGB:0.04Ce^{3+},yTb^{3+} phosphors was tuned from blue light (0.164, 0.042) to green light (0.331, 0.485) when the concentration y increased from 0.00 to 0.50. In addition, the IQE of CLGB:0.04Ce^{3+},0.25Tb^{3+} reached as high as 57.9%. The temperature-dependent spectra of CLGB:0.04Ce^{3+},0.40Tb^{3+} sample revealed that the as-prepared phosphor had good thermal stability with activation energy ΔE of 0.3142 eV. The fabricated prototype w-LED device showed good photoelectric properties with CIE chromaticity coordinates of (0.3996, 0.3856), Ra = 81.2, and CCT = 3588 K. All the results suggest that CLGB:Ce^{3+},Tb^{3+} phosphors have potential for application in w-LEDs as a color-tunable phosphor.

Conflicts of interest

There are no conflicts to declare.

Acknowledgements

The present research work was supported by the National Natural Science Foundation of China (No. 51502190), the Program for the Outstanding Innovative Teams of Higher Learning Institutions of Shanxi, the Start-up Research Grant of Taiyuan University of Technology (No. Tyut-rc201489a), the Excellent Young Scholars Research Grant of Taiyuan University of Technology (No. 2014YQ009, 2015YQ006, and 2016YQ03), and the Open Fund of the State Key Laboratory of Luminescent Materials and Devices (South China University of Technology, No. 2017-skllmd-01).

References

1 M. Jiao, Q. Xu, C. Yang and H. You, *RSC Adv.*, 2017, **7**, 28647–28654.
2 C. C. Lin, A. Meijerink and R. S. Liu, *J. Phys. Chem. Lett.*, 2016, **7**, 495–503.
3 S. Liang, M. Shang, H. Lian, K. Li, Y. Zhang and J. Lin, *J. Mater. Chem. C*, 2016, **4**, 6409–6416.
4 M. Peng, X. Yin, P. A. Tanner, M. G. Brik and P. Li, *Chem. Mater.*, 2015, **27**, 2938–2945.

5 J. Zhong, D. Chen, H. Xu, W. Zhao, J. Sun and Z. Ji, *J. Alloys Compd.*, 2017, **695**, 311–318.
6 H. Guo, X. Huang and Y. Zeng, *J. Alloys Compd.*, 2018, **741**, 300–306.
7 X. Huang, B. Li and H. Guo, *Ceram. Int.*, 2017, **43**, 10566–10571.
8 L. Li, Y. Pan, Y. Huang, S. Huang and M. Wu, *J. Alloys Compd.*, 2017, **724**, 735–743.
9 W. Dai, Y. Lei, J. Zhou, Y. Zhao, Y. Zheng, M. Xu, S. Wang and F. Shen, *J. Am. Ceram. Soc.*, 2017, **100**, 5174–5185.
10 R. Cao, T. Fu, Y. Cao, H. Ao, S. Guo and G. Zheng, *Mater. Lett.*, 2015, **155**, 68–70.
11 M. Hermus, P.-C. Phan and J. Brgoch, *Chem. Mater.*, 2016, **28**, 1121–1127.
12 P. Du, X. Huang and J. S. Yu, *Chem. Eng. J.*, 2018, **337**, 91–100.
13 H. Zhang, X. Zhang, Z. Cheng, Y. Xu, J. Yang and F. Meng, *Ceram. Int.*, 2018, **44**, 2547–2551.
14 X. Huang, B. Li, H. Guo and D. Chen, *Dyes Pigm.*, 2017, **143**, 86–94.
15 J. Han, L. Li, M. Peng, B. Huang, F. Pan, F. Kang, L. Li, J. Wang and B. Lei, *Chem. Mater.*, 2017, **29**, 8412–8424.
16 X. Huang, *Nat. Photonics*, 2014, **8**, 748–749.
17 H. Xu, Z. Zhou, Y. Liu, Q. Liu, Z. He, S. Wang, L. Huang and H. Zhu, *Luminescence*, 2017, **32**, 812–816.
18 P. Du, L. Krishna Bharat and J. S. Yu, *J. Alloys Compd.*, 2015, **633**, 37–41.
19 R. Shi, J. Xu, G. Liu, X. Zhang, W. Zhou, F. Pan, Y. Huang, Y. Tao and H. Liang, *J. Phys. Chem. C*, 2016, **120**, 4529–4537.
20 P. Xu, Z. Fu, S. Fan, H. Lin, C. Li, G. Yao, Q. Chen, Y. Zhou and F. Zeng, *J. Non-Cryst. Solids*, 2018, **481**, 441–446.
21 A. Huang, Z. Yang, C. Yu, Z. Chai, J. Qiu and Z. Song, *J. Phys. Chem. C*, 2017, **121**, 5267–5276.
22 M. Zhao, Z. Zhao, L. Yang, L. Dong, A. Xia, S. Chang, Y. Wei and Z. Liu, *J. Lumin.*, 2018, **194**, 297–302.
23 F. Kang, H. Zhang, L. Wondraczek, X. Yang, Y. Zhang, D. Y. Lei and M. Peng, *Chem. Mater.*, 2016, **28**, 2692–2703.
24 P. Ma, B. Yuan, Y. Sheng, K. Zheng, Y. Wang, C. Xu, H. Zou and Y. Song, *J. Alloys Compd.*, 2017, **714**, 627–635.
25 X. Wu, Y. Jiao, O. Hai, Q. Ren, F. Lin and H. Li, *J. Alloys Compd.*, 2018, **730**, 521–527.
26 Y. Li, W. Chen, L. Zhao, D. Meng, Y. Zhang and C. Wang, *New J. Chem.*, 2017, **41**, 14876–14881.
27 S. A. Khan, W. Ji, L. Hao, X. Xu, S. Agathopoulos and N. Z. Khan, *Opt. Mater.*, 2017, **72**, 637–643.
28 M. Ding, M. Xu and D. Chen, *J. Alloys Compd.*, 2017, **713**, 236–247.
29 H. Guo, B. Devakumar, B. Li and X. Huang, *Dyes Pigm.*, 2018, **151**, 81–88.
30 D. Wu, W. Xiao, L. Zhang, X. Zhang, Z. Hao, G.-H. Pan, Y. Luo and J. Zhang, *J. Mater. Chem. C*, 2017, **5**, 11910–11919.
31 F. Du, W. Zhuang, R. Liu, Y. Liu, J. Zhong, P. Gao, X. Zhang, W. Gao and L. Shao, *RSC Adv.*, 2017, **7**, 1075–1081.
32 H. Xu, Q. Liu, L. Huang, Z. He, S. Wang, C. Jiang and Q. Peng, *Opt. Laser Technol.*, 2017, **89**, 151–155.
33 K. Li, H. Lian, Y. Han, M. Shang, R. Van Deun and J. Lin, *Dyes Pigm.*, 2017, **139**, 701–707.
34 B. Li, X. Huang, H. Guo and Y. Zeng, *Dyes Pigm.*, 2018, **150**, 67–72.
35 H. N. Luitel, R. Chand and T. Watari, *Adv. Condens. Matter Phys.*, 2015, **2015**, 1–9.
36 S. Xu, Z. Wang, P. Li, T. Li, Q. Bai, J. Sun and Z. Yang, *J. Am. Ceram. Soc.*, 2017, **100**, 2069–2080.
37 H. Huang, X. Feng, T. Chen, Y. Xiong and F. Zhang, *Luminescence*, 2018, **33**, 692–697.
38 X. Li, C. Liu, L. Guan, W. Wei, Z. Yang, Q. Guo and G. Fu, *Mater. Lett.*, 2012, **87**, 121–123.
39 S.-Z. Ma, W.-L. Feng, R. Chen and Z.-Q. Peng, *J. Alloys Compd.*, 2017, **700**, 49–53.
40 D. Wen, H. Kato, M. Kobayashi, S. Yamamoto, M. Mitsuishi and M. Kakihana, *J. Mater. Chem. C*, 2017, **5**, 4578–4583.
41 M. Ding, H. Zhang, D. Chen, Q. H. Junhua Xi and Z. Ji, *J. Alloys Compd.*, 2016, **672**, 117–124.
42 M. Ding, J. Hou, Z. Cui, H. Gao, C. Lu, J. Xi, Z. Ji and D. Chen, *Ceram. Int.*, 2018, **44**, 7930–7938.
43 R. Yu, H. M. Noh, B. K. Moon, B. C. Choi, J. H. Jeong, K. Jang, H. S. Lee and S. S. Yi, *Mater. Res. Bull.*, 2014, **51**, 361–365.
44 C.-Y. Wang, O. M. t. Kate, T. Takeda and N. Hirosaki, *J. Mater. Chem. C*, 2017, **5**, 8295–8300.
45 M. Hermus, P.-C. Phan, A. C. Duke and J. Brgoch, *Chem. Mater.*, 2017, **29**, 5267–5275.
46 J. Sun, Y. Sun, J. Zeng and H. Du, *J. Phys. Chem. Solids*, 2013, **74**, 1007–1011.
47 N. Guo, Y. Song, H. You, G. Jia, M. Yang, K. Liu, Y. Zheng, Y. Huang and H. Zhang, *Eur. J. Inorg. Chem.*, 2010, **2010**, 4636–4642.
48 E. Cavalli, P. Boutinaud, R. Mahiou, M. Bettinelli and P. Dorenbos, *Inorg. Chem.*, 2010, **49**, 4916–4921.
49 X. Huang, B. Li and H. Guo, *J. Alloys Compd.*, 2017, **695**, 2773–2780.
50 G. V. Lokeswara Reddy, L. Rama Moorthy, P. Packiyaraj and B. C. Jamalaiah, *Opt. Mater.*, 2013, **35**, 2138–2145.
51 M. Xin, D. Tu, H. Zhu, W. Luo, Z. Liu, P. Huang, R. Li, Y. Cao and X. Chen, *J. Mater. Chem. C*, 2015, **3**, 7286–7293.
52 Y. Zhang, H. Liu, L. Mei, M. S. Molokeev, Y. Wang and Z. Huang, *J. Solid State Chem.*, 2017, **255**, 36–41.
53 B. P. Kore, S. Tamboli, N. S. Dhoble, A. K. Sinha, M. N. Singh, S. J. Dhoble and H. C. Swart, *Mater. Chem. Phys.*, 2017, **187**, 233–244.
54 C. H. Huang, T. W. Kuo and T. M. Chen, *ACS Appl. Mater. Interfaces*, 2010, **2**, 1395–1399.
55 G.-G. Wang, X.-F. Wang, L.-W. Dong and Q. Yang, *RSC Adv.*, 2016, **6**, 42770–42777.
56 A. Guan, P. Chen, L. Zhou, G. Wang, X. Zhang and J. Tang, *Spectrochim. Acta, Part A*, 2017, **173**, 53–58.
57 C.-H. Huang, W.-R. Liu, T.-W. Kuo and T.-M. Chen, *Chem*, 2011, **1**, 9–15.
58 G. Mo, Z. Wei, L. Ma and G. Wen, *J. Mater. Sci.: Mater. Electron.*, 2016, **28**, 2557–2562.
59 J. Zhou and Z. Xia, *J. Mater. Chem. C*, 2015, **3**, 7552–7560.
60 H.-L. Lai, R.-Y. Yang and S.-J. Chang, *Ceram. Int.*, 2017, **43**, S688–S693.
61 Z. Xia and R.-S. Liu, *J. Phys. Chem. C*, 2012, **116**, 15604–15609.

62 B. Wang, Y.-g. Liu, Z. Huang and M. Fang, *Chem. Phys. Lett.*, 2017, **690**, 31–37.
63 J. Huo, W. Lü, B. Shao, Y. Feng, S. Zhao and H. You, *Dyes Pigm.*, 2017, **139**, 174–179.
64 Z. Jia and M. Xia, *New J. Chem.*, 2017, **41**, 12416–12421.
65 X. Zhang, J. Zhang and Y. Chen, *Dyes Pigm.*, 2018, **149**, 696–706.
66 F. Kang, M. Peng, D. Y. Lei and Q. Zhang, *Chem. Mater.*, 2016, **28**, 7807–7815.